Thermochimica Acta 483 (2009) 55–57

Contents lists available at ScienceDirect

Thermochimica Acta

journal homepage: www.elsevier.com/locate/tca

Subsolidus phase diagram of binary system of thermotropic phase transitions compounds (n-$C_nH_{2n+1}NH_3)_2MnCl_4$ (n = 12, 14, 16)

Kezhong Wu*, Jianjun Zhang, Xiaodi Liu

Department of Chemistry and Material Science, Key Laboratory of Inorganic Nano-materials of Hebei Province, Hebei Normal University, 113 YuHua Rd., Shijiazhuang 050016, China

ARTICLE INFO

Article history:
Received 22 September 2008
Received in revised form 5 November 2008
Accepted 7 November 2008
Available online 19 November 2008

Keywords:
Dodecylammonium tetrachloromanganate
Tetradecylammonium tetrachloromanganate
Hexadecylammonium tetrachloromanganate
Phase diagram

ABSTRACT

The thermotropic phase transitions in the perovskite type layer compound (n-$C_nH_{2n+1}NH_3)_2$ $MnCl_4$ (n = 12, 14, 16) were studied and a series of their mixtures were prepared. The low temperature crystal structures of the pure salts are characteristic of the piling of sandwiches in which a two-dimensional macro-anion $MnCl_4^{2-}$ is sandwiched between two alkylammonium layers. These layers become conformationally disordered in the high temperature phases. The subsolidus binary phase diagrams of (n-$C_{12}H_{25}NH_3)_2MnCl_4$–($n$-$C_{14}H_{29}NH_3)_2MnCl_4$ and (n-$C_{14}H_{29}NH_3)_2MnCl_4$–($n$-$C_{16}H_{33}NH_3)_2MnCl_4$ were established by differential thermal analysis (DTA) and X-ray diffraction (XRD). In each phase diagram, an intermediate compound and two eutectoid invariants were observed. There are three noticeable solid solution ranges (α, β, γ) at the left boundary, right boundary and middle of the phase diagram.

1. Introduction

The investigation of perovskite type layer compounds with the general formula (n-$C_nH_{2n+1}NH_3)_2MCl_4$ (M = Cu, Mn, Cd, Zn, Co, etc.) (short notation; C_nM) has greatly contributed to our understanding of phase transitions in layer structures. The advances in synthesis along with the ease of controlling various structural parameters (metal, halogen and number of carbon atoms in the alkylammonium ion) have made them ideal objects for studies by spectroscopy, calorimetry, diffraction, and a variety of other techniques [1,2]. In the case of C_nMn, parallel sheets of corner-sharing $MnCl_6$ octahedral are held together by the n-alkylammonium groups. The $-NH_3^+$ groups of the chains occupy the cavities of the $MnCl^{2-}$ layers and are bonded by hydrogen bonds to the chlorine atoms. The physical properties and structures of C_nM [3–7] have been previously researched. The binary phase diagrams for $C_{10}Zn$–$C_{12}Zn$ [8], $C_{10}Zn$–$C_{16}Zn$ [9,10], $C_{12}Zn$–$C_{16}Zn$ [9,10], $C_{12}Zn$–$C_{18}Zn$ [11], $C_{10}Co$–$C_{16}Co$ [10], $C_{12}Co$–$C_{16}Co$ [10,12], $C_{12}Mn$–$C_{16}Mn$ [13,14] have been reported. Among them, $C_{10}Zn$–$C_{16}Zn$ [10], $C_{12}Mn$–$C_{16}Mn$ [13], $C_{10}Co$–$C_{16}Co$ [10,12] and $C_{12}Co$–$C_{16}Co$ [10] show absolute immiscibility. As we know, the binary phase diagrams of $C_{12}Mn$–$C_{14}Mn$ and $C_{14}Mn$–$C_{16}Mn$ have not been studied. In this work we synthesized three types of materials of $[NR_4]_2MnCl_4$ in bis(n-alkylammonium) tetrachloromanganate(II) with the general formula (n-$C_{12}H_{25}NH_3)_2MnCl_4$ (short notation; $C_{12}Mn$), (n-$C_{14}H_{29}NH_3)_2MnCl_4$ ($C_{14}Mn$) and (n-$C_{16}H_{33}NH_3)_2MnCl_4$ ($C_{16}Mn$). The phase diagrams of $C_{12}Mn$–$C_{14}Mn$ and $C_{14}Mn$–$C_{16}Mn$ were established by differential thermal analysis (DTA) and X-ray diffraction (XRD).

2. Experimental procedure

$MnCl_2$, concentrated HCl and absolute ethanol were analytical grade. Dodecylamine (C.P.) was purchased from Tianjin Xiqing Kelong Reagent Plant (China), tetradecylamine (A.P.) was purchased from TOKYO KASEI KOGYO Co. Ltd. (Japan) and hexadecylamine (A.P.) was purchased from ACROS ORGANICS (Germany).

For the synthesis of C_nMn, the hot absolute ethanol solutions of $MnCl_2$, concentrated HCl and the corresponding alkylamine were mixed in a 1:2:2 molar ratio. The solutions were concentrated by boiling for 30 min, then cooled to room temperature. After filtration, the products were recrystallized twice from absolute ethanol. Finally, they were placed in a vacuum desiccator for 8 h at about 353 K. $C_{12}Mn$, $C_{14}Mn$ and $C_{16}Mn$ were analyzed with an MT-3 CHN elemental analyzer (Japan). Elemental analysis calc. (%) for $C_{12}Mn$: C 50.62, H 9.84, N 4.92; found: C 50.69, H 10.08, N 4.69. Anal. calc. (%) for $C_{14}Mn$: C 53.76, H 9.28, N 4.48; found: C 54.18, H 10.42, N 4.53; Anal. calc. (%) for $C_{16}Mn$: C 56.38, H 10.57, N 4.11; found: C 56.46, H 10.81, N 3.85. The C_nMn samples were weighed exactly in the desired proportions to prepare the mixed samples of $C_{12}Mn$–$C_{14}Mn$

* Corresponding author. Tel.: +86 311 86268049.
E-mail address: wukzh688@163.com (K. Wu).

0040-6031/$ – see front matter © 2008 Elsevier B.V. All rights reserved.
doi:10.1016/j.tca.2008.11.002

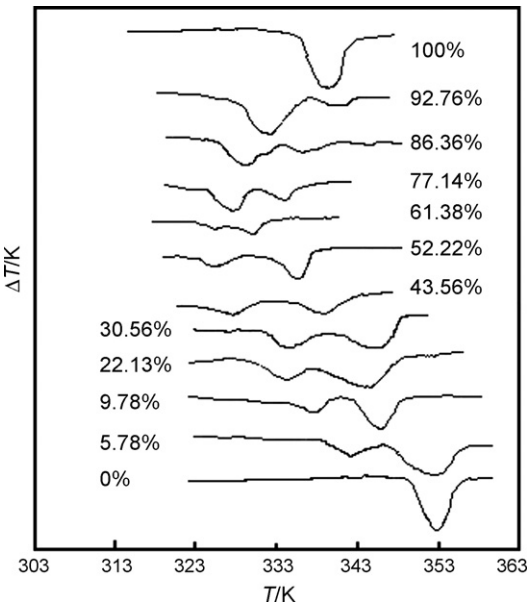

Fig. 1. DTA curves of $C_{14}Mn$–$C_{16}Mn$ with different $W_{C_{14}Mn\%}$.

and $C_{14}Mn$–$C_{16}Mn$. The two components were dissolved in absolute ethanol, then the solvent was evaporated. The samples were dried in a vacuum desiccators for 8 h at a temperature of about 253 K. The concentrations of $C_{14}Mn$ in the binary system was expressed as $W_{C_{14}Mn\%}$.

The DTA curve was measured on a CDR-4P differential scanning calorimeter (DTA; Shanghai Scale Instrument Plant) at a scanning rate of 5 K/min in a static atmosphere. Samples of about 4.5 mg were sealed in aluminum crucibles. X-ray diffraction patterns of the powders were taken with a D/MAX-RA X-ray diffractometer (made in Japan) using Cu Kα radiation (Ni filter) at a scanning rate of 2 min^{-1}. The voltage and electric current were 40 kV and 100 mA, respectively.

3. Results and discussion

3.1. Thermal analysis

Fig. 1 shows some typical DTA curves of $C_{14}Mn$–$C_{16}Mn$ binary systems with different $W_{C_{14}Mn\%}$. The results of the DTA experiments obtained using the "Shape factors method" [15] are listed in Table 1. All the $C_{14}Mn$–$C_{16}Mn$ binary systems show solid–solid phase transitions in the temperature range 319–360 K. The data in Table 1 show that the value of the transition temperature decreases with increasing $W_{C_{14}Mn\%}$ in the range from 0 to 19.90%. Then, the phase transition temperature first rises from $W_{C_{14}Mn\%}$ 19.90 to 33.75%. The first eutectoid temperature (about 329.6 K) appears in the $W_{C_{14}Mn\%}$ range 14.68–30.56%. The phase transition temperature decreases again from $W_{C_{14}Mn\%}$ 33.75 to 67.71%, and then rises with the increasing $W_{C_{14}Mn\%}$. The second eutectoid temperature at about 319.7 K was found in the $W_{C_{14}Mn\%}$ range of 47.12–73.18%. Table 1 reveals that the first eutectoid temperature is not close to that pure $C_{16}Mn$ $W_{C_{14}Mn\%} = 0$, nor does the second eutectoid temperature end near that pure $C_{14}Mn$ $W_{C_{14}Mn\%} =$ 100%. The range of the first eutectoid temperature does not end close to the beginning of the second eutectoid temperature. It is clear that the phase transition temperatures of the binary system $C_{14}Mn$–$C_{16}Mn$ in solid–solid phase transitions show a strong dependence on $W_{C_{14}Mn\%}$. The reason is that there are not only intermediates of the form $(n\text{-}C_{14}H_{29}NH_3)(n\text{-}C_{16}H_{33}NH_3)\,MnCl_4$ (short notation; $C_{14}C_{16}Mn$) but also three solid solution ranges existing at the left boundary, right boundary and middle of the phase diagram of $C_{14}Mn$–$C_{16}Mn$.

Table 1
Solid–solid transition temperatures for the $C_{14}Mn$–$C_{16}Mn$ binary systems with different $W_{C_{14}Mn\%}$.

$W_{C_{14}Mn\%}$	T_{e1}/K	T_{e2}/K	T_{s1}/K	T_{s2}/K
0 ($C_{16}Mn$)				349.8
5.78			338.2	346.0
9.78			333.0	344.1
12.93			330.2	339.8
18.23	329.6			334.0
22.13	329.6			336.6
26.84	329.6			338.6
30.56	329.6			340.0
36.18			326.5	339.8
43.36			321.0	336.3
47.12		319.7		334.1
52.22		320.3		332.1
55.71		319.7		328.8
61.38		319.7		327.2
64.83		319.7		323.4
70.19		319.7		323.6
73.18		320.3		328.8
77.14			321.1	329.1
80.45			322.2	330.8
86.36			324.7	332.6
89.85			325.8	335.6
92.76			327.2	336.3
95.36			329.6	336.1
100 ($C_{14}Mn$)				336.3

Note: T_e, eutectoid invariant; T_s, solid–solid transition temperature.

3.2. X-ray diffraction

Fig. 2 shows the X-ray diffraction patterns at room temperature for pure $C_{14}Mn$, $C_{16}Mn$ and their binary systems. The diffraction patterns of the sample with $W_{C_{14}Mn\%}$ 9.78% is similar to that of pure $C_{16}Mn$, indicating a single-phase region. In this concentration range, $C_{14}C_{16}Mn$ dissolves in $C_{16}Mn$ to form a solid solution α. Similarly, samples with $W_{C_{14}Mn\%}$ from 95.39% to pure $C_{14}Mn$ have homologous patterns, revealing that the $C_{14}C_{16}Mn$ dissolves in $C_{14}Mn$ to form a solid solution β. In the same way, $C_{14}Mn$–$C_{16}Mn$ samples with $W_{C_{14}Mn\%}$ from 30.56 to 47.12% have similar diffraction patterns, showing that $C_{14}Mn$ or $C_{16}Mn$ dissolved in $C_{14}C_{16}Mn$ forms a single-phase γ. $C_{14}Mn$–$C_{16}Mn$ samples with $W_{C_{14}Mn\%}$ from 14.68 to 30.56% are in the two-phase region, and their patterns are an overlap of α and γ. The X-ray diffraction patterns of $C_{14}Mn$–$C_{16}Mn$ samples with the $W_{C_{14}Mn\%}$ range of 47.12–73.18% are an overlap of β and γ and thus in the two-phase region.

3.3. Establishment of phase diagram

The binary phase diagram of $C_{14}Mn$–$C_{16}Mn$ (Fig. 3) was obtained according to the temperature–composition relations from the DTA and X-ray diffraction experiments. Fig. 3 indicates that an intermediate compound $(n\text{-}C_{14}H_{29}NH_3)_{2/3}(n\text{-}C_{16}H_{33}NH_3)_{1/3}MnCl_4$ is formed between two eutectoid invariants [16]. The low temperature perovskite-layer structure of $C_{14}Mn$, $C_{16}Mn$ and their binary system are organized by neutralizing $MnCl_4^{2-}$ with alkylammonium ions. Alkylammonium chains lie parallel to each other and are slightly tilted with respect to the normal of the inorganic layers. The adjacent alkyl chains interact with each other by van der Waals interactions, and are hydrogen bonded to $MnCl_4^{2-}$. When the temperature is increased to 329.6 K, the first eutectoid invariant occurs from $W_{C_{14}Mn\%}$ 14.68 to 30.56%. $C_{16}Mn$ and $C_{14}C_{16}Mn$ undergo a reversible solid–solid phase transformation. In this situation, the chains possess a large degree of motional freedom and a disordered

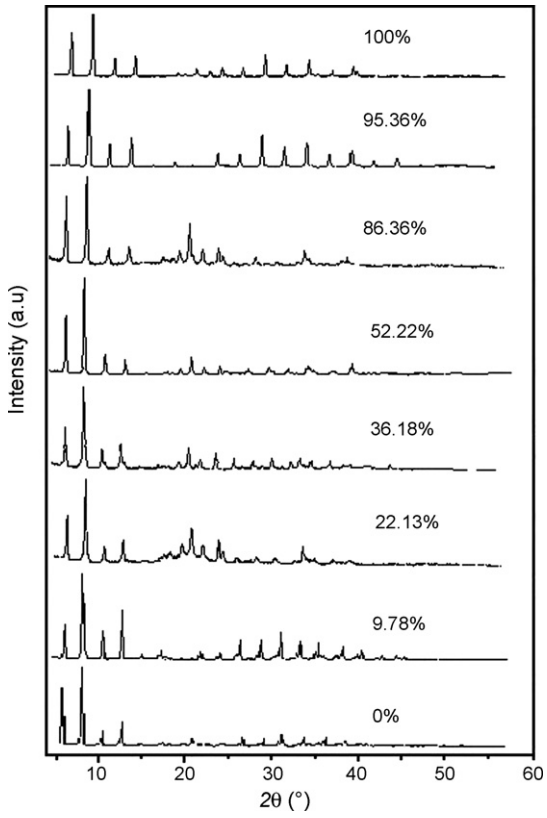

Fig. 2. The diffraction patterns for $C_{14}Mn$, $C_{16}Mn$ and their binary systems with different $W_{C_{14}Mn\%}$.

phase appears. At the same time, the hydrogen bonds are weakened and even destroyed. The second eutectoid invariant appears from $W_{C_{14}Mn\%}$ 47.12 to 73.18% at 319.7 K. Similarly, $C_{14}Mn$ and $C_{14}C_{16}Mn$ undergo a reversible solid–solid phase transformation.

The binary phase diagram of $C_{12}Mn$–$C_{14}Mn$ was obtained in the same way (*see* Fig. 4). The first eutectoid temperature 313 K appears in the $W_{C_{14}Mn\%}$ range from 13.25 to 35.52%. The second eutectoid temperature at about 313 K was found in the $W_{C_{14}Mn\%}$ range from 59.64 to 74.80%. Simultaneously, an intermediate compound (n-$C_{12}H_{25}NH_3$)(n-$C_{14}H_{29}NH_3$)$MnCl_4$ ($C_{12}C_{14}Mn$) and two eutectoid invariants were observed. There are three noticeable solid solution ranges (α, β, γ) at the left boundary, right boundary and middle of the phase diagram. The phase diagrams of $C_{14}Mn$–$C_{16}Mn$ and $C_{12}Mn$–$C_{14}Mn$ obtained in this work are similar to that of $C_{12}Mn$–$C_{16}Mn$ which has been reported in our previous work [14]. For $C_{12}Mn$–$C_{14}Mn$ and $C_{12}Mn$–$C_{16}Mn$ systems, the molar ratio between the two n-alkylammonium groups of the intermediate compound is both 1:1, while it is 2:1 for the intermediate compound (n-$C_{14}H_{29}NH_3$)$_{2/3}$(n-$C_{16}H_{33}NH_3$)$_{1/3}MnCl_4$ of the $C_{14}Mn$–$C_{16}Mn$ binary system. It is worth noting that our phase diagrams are different from those of the other homologous systems $C_{10}Zn$–$C_{16}Zn$ [10], $C_{12}Mn$–$C_{16}Mn$ [13], $C_{10}Co$–$C_{16}Co$ [10,12] and $C_{12}Co$–$C_{16}Co$ [10]. The most remarkable difference is that these phase diagrams show absolute immiscibility, while partial miscibility was observed in this work.

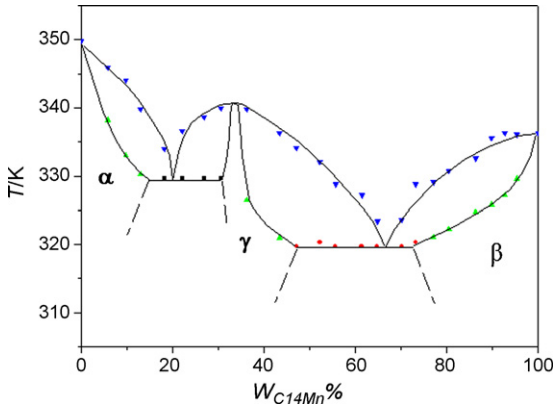

Fig. 3. Phase diagram of the $C_{14}Mn$–$C_{16}Mn$ system.

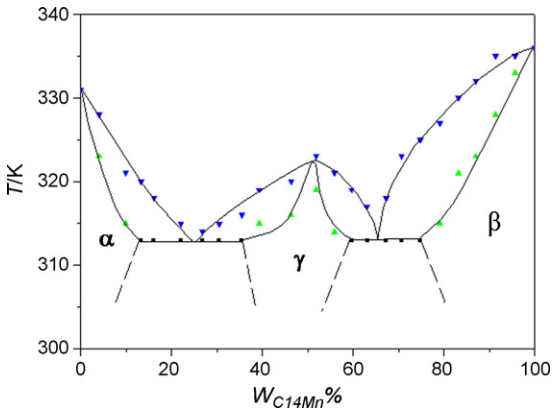

Fig. 4. Phase diagram of the $C_{12}Mn$–$C_{14}Mn$ system.

4. Conclusion

The binary phase diagrams of $C_{14}Mn$–$C_{16}Mn$ and $C_{12}Mn$–$C_{14}Mn$ mixtures were established by DTA and XRD. Their phase diagrams are very similar, belonging to a partially miscible system. Intermediate compounds of (n-$C_{14}H_{29}NH_3$)$_{2/3}$(n-$C_{16}H_{33}NH_3$)$_{1/3}MnCl_4$ and (n-$C_{12}H_{25}NH_3$)(n-$C_{14}H_{29}NH_3$)$MnCl_4$ were observed in $C_{14}Mn$–$C_{16}Mn$ and $C_{12}Mn$–$C_{14}Mn$ system, respectively. There are three noticeable solid solution ranges, at the left boundary, right boundary, and middle of the phase diagram. It is revealed that the crystal structure and the size of the molecule are the essential factors that affect the miscibility of the binary systems.

Acknowledgements

This project was financially supported by National Natural Science Foundation of China (No. 20773034), Natural Science Foundation of Hebei Province (No. B2007000237), Education Department Scientific Research Fund from Hebei Province (2008469) and Science Foundation of Hebei Normal University (L2006B16, L2007Q16).

References

[1] K.J. Schenk, G. Chapuis, J. Phys. Chem. 92 (1988) 7141–7147.
[2] N.V. Venkataraman, S. Barman, S. Vasudevan, Chem. Phys. Lett. 358 (2002) 139–143.
[3] Y. Tabuchi, K. Asai, M. Rikukawa, J. Phys. Chem. Solids 61 (2000) 837–845.
[4] J. Fenrych, E.C. Reynhardt, S. Jurga, et al., Mol. Phys. 78 (1993) 1117–1128.
[5] R.Y. Xu, D.J. Kong, X.E. Cai, et al., Thermochim. Acta 164 (1990) 307–314.
[6] K.Z. Wu, J.L. Li, J.J. Zhang, X.D. Liu, Chin. J. Chem. 26 (2008) 216–219.
[7] V. Busico, T. Tartaglione, M. Vacatello, Thermochim. Acta 62 (1983) 77–86.
[8] K.Z. Wu, P. Zuo, X.D. Liu, Y.J. Li, Thermochim. Acta 397 (2003) 49–53.
[9] K.Z. Wu, C.X. Zhang, Y.J. Li, X.D. Liu, J. Chin. Chem. Soc. 52 (2005) 45–50.
[10] D.S. Ruan, W.P. Li, L.F. He, Q.H. Hu, J. Therm. Anal. 45 (1995) 235–242.
[11] K.Z. Wu, X.D. Wang, X.D. Liu, J. Univ. Sci. Technol. Beijing 10 (2003) 75–77.
[12] W.P. Li, D.S. Zhang, T.P. Zhang, et al., Thermochim. Acta 326 (1999) 183–186.
[13] V. Salerno, A. Grieco, M. Vacatello, J. Phys. Chem. 80 (1976) 2444–2448.
[14] K.Z. Wu, W.Z. Cui, J.J. Zhang, Thermochim. Acta 463 (2007) 15–17.
[15] R. Courchinoux, N.B. Chanh, Y. Haget, Thermochim. Acta 128 (1988) 45–53.
[16] P.W. Atkins, Physical Chemistry, Oxford University, Oxford, 1990.